1 Mathematical Modeling of CO₂ Facilitated Transport across Polyvinylamine

2 Membranes with Direct *Operando* Observation of Amine Carrier Saturation

- 3 Hui Xu, ¹ Sarah G. Pate, ² and Casey P. O'Brien²*
- ¹Department of Chemistry and Biochemistry, University of Notre Dame, Notre Dame, IN, 46556, United States.
- 5 ²Department of Chemical and Biomolecular Engineering, University of Notre Dame, Notre Dame, IN, 46556, United
- 6 States.

7

8

9

10

11

12

13

14

15

16

17

18

19

20

21

22

Abstract

In this work, we investigate the kinetics and mechanisms of CO₂ facilitated transport across polyvinylamine (PVAm) membranes using mathematical modeling of experimentally measured CO₂ fluxes across PVAm with operando surface-enhanced Raman spectroscopic (SERS) and Fourier-transform infrared (FTIR) spectroscopy characterization. The mathematical model was fit to experimentally measured CO₂ fluxes as a function of CO₂ partial pressure (2-99 kPa) and PVAm membrane thickness (1.7-4.1 µm). Physically significant kinetic and thermodynamic parameters associated with CO₂ transport were extracted from the model, such as the permeability of PVAm to CO₂ via solution diffusion, the permeability of PVAm to carbamate (NHCOO⁻) via facilitated transport, and the carbamate formation/decomposition equilibrium constant. Our results show that the permeability of PVAm to carbamate via facilitated transport (2200 ± 1200 Barrer) is about an order of magnitude greater than the permeability of PVAm to CO₂ via solution-diffusion of CO₂ $(150 \pm 20 \, \text{Barrer})$. Using operando SERS and FTIR, we directly observed saturation of the primary amine groups of PVAm with CO₂ (carbamate) at a feed CO₂ partial pressure of ~10 kPa, which was in good agreement with our model predictions. This work quantitatively describes CO₂ facilitated transport across PVAm and provides direct evidence of the carrier saturation

phenomenon—for the first time to our knowledge—from a molecular perspective through operando spectroscopic characterization. Keywords: Facilitated transport, Membrane separations, Mathematical modeling, CO₂ capture, Operando spectroscopy

1. Introduction

Separating CO₂ from other gases, such as N₂ and CH₄, has become increasingly important to combat climate change and for natural gas processing [1]. Conventional CO₂ separation technologies such as amine scrubbing can separate CO₂ from mixed gases with high selectivity [2-4] and can produce nearly-pure CO₂ streams. However, these processes are extremely inefficient and expensive because they require energy intensive temperature-swing regeneration stages to release CO₂ and regenerate the sorbent [5]. Membrane-based CO₂ separation is an attractive alternative, because it is intrinsically a continuous process, hence requiring a smaller footprint and simpler setup/operation than sorbent-based CO₂ capture [1, 6, 7]. Amine-based membranes in particular have attracted a great deal of attention for CO₂ capture from concentrated point sources such as flue gas, where various pre-pilot and pilot-scale field tests have been carried out [8-11]. They are also promising for CO₂ capture from dilute sources such as air because of their unique facilitated CO₂ transport mechanism.

In amine-based facilitated transport membranes (FTMs), amine carriers in the membrane selectively enhance the transport of CO₂ without affecting the transport of other gases that follow the solution-diffusion mechanism (e.g., N₂ and CH₄), which results in CO₂ permeances and selectivities that can exceed the "upper bound" inherent to polymeric membranes [12-16]. Due to the high proportion of free amine groups in the membrane that are unoccupied at low CO₂ partial pressures, these FTMs exhibit the highest permeances and selectivities at low CO₂ partial pressures [12, 17-20]. This unique property of FTMs makes them attractive for capturing CO₂ from dilute sources, such as air [21, 22]. When the amine sites become saturated with CO₂, any further increase in the CO₂ partial pressure only increases the CO₂ flux via solution diffusion [23-26]. To our knowledge, amine carrier saturation has never been directly observed. Instead, evidence of

facilitated transport is frequently cited as the observation that the apparent CO₂ permeance decreases with increasing CO₂ partial pressure until reaching a constant value [17, 26]. We introduce the term 'apparent CO₂ permeance' here to emphasize that the CO₂ permeance typically reported in the literature [27, 28] for FTMs is a convolution of two different transport mechanisms—facilitated transport and solution diffusion—with different intrinsic permeances.

Although various amine-based FTMs have been investigated for CO₂ separation, the membrane performance has received the majority of the focus, while aspects related to the understanding of facilitated transport still need to be clarified. To clarify transport mechanisms, we have developed *operando* spectroscopy tools to monitor the membrane structural changes resulting from CO₂ transport across the membrane [29, 30]. As CO₂ passes through the PVAm membrane, these tools have made it possible to identify carbamate (*NHCOO*⁻) intermediates in polyvinylamine (PVAm) [29, 30]. Although we have identified the CO₂ transport intermediate for PVAm, there are still many unsolved questions: (1) What is the intrinsic permeability of CO₂ via facilitated transport compared to the solution-diffusion of neutral CO₂? (2) What is the relative flux of CO₂ via facilitated transport of carbamate compared to that of solution diffusion of neutral CO₂? (3) At what CO₂ partial pressures do the amine sites saturate? This work addresses these questions by mathematical modeling of CO₂ transport and *operando* observation of carbamate formation as a function of CO₂ partial pressure and PVAm membrane thickness.

Some mathematical models have been developed to investigate facilitated transport based on simplified solutions that approximate the actual membrane behavior [17, 31-35]. Han et al. explained the dependence of CO₂ permeance on CO₂ partial pressure by describing the facilitated transport membrane with a homogeneous reactive diffusion model [35], where it was assumed that CO₂ reacts reversibly with amine carriers in the membrane and diffuses across the membrane as

bicarbonate (HCO₃) [17, 36]. Yang et al. developed a mathematical model using a tanks-in-series approach to study the FTMs and took into account the simultaneous effects of relative humidity (RH%), temperature, and CO₂ partial pressure [31, 32]. Some researchers have attempted to model the facilitated transport system using the dual-mode (DM) transport model [37-44], which describes the equilibrium concentration of solutes in glassy polymers as a sum of the concentration of gas dissolved in the polymer matrix (Henry's law [45]) and the concentration of gas adsorbed in the holes of the polymer matrix (Langmuir sorption [37]) [46]. Although the dual-mode (DM) transport model fits well for many fixed site carrier systems, there is no clear and comprehensive interpretation of the transport mechanism, particularly the chemical reactions, in these FTMs. Cussler et al. [47] and Noble et al. [42-44] derived phenomenological models to consider the role of chemical reactions and polymer morphology in facilitated transport of CO₂.

As a continuation of our previous work [29, 30], a simple CO₂ transport mathematical model is proposed here. Unlike previous modeling studies [17, 31, 32, 35-44, 47] that have focused primarily on modeling membrane performance, the model proposed here was developed with the aim gaining more fundamental and quantitative insight into the transport mechanism. The model was fit to CO₂ fluxes measured across PVAm membranes as a function of feed CO₂ partial pressure (2-99 kPa) and membrane thickness (1.7-4.1 µm). Fundamental kinetic and thermodynamic parameters associated with CO₂ transport across PVAm were extracted from the model, such as the intrinsic permeability of CO₂ via facilitated transport, the intrinsic permeability of CO₂ via solution-diffusion, and carbamate formation/decomposition equilibrium constant. We also used *operando* Raman and FTIR spectroscopy in parallel to study the changes to the membrane structure while CO₂ transports across PVAm under varied CO₂ feed partial pressures. We observed that as the feed CO₂ partial pressure increases, the band intensities associated with

carbamate species also increase and reach a saturation point at ~10 kPa CO₂ where no further increases in band intensities are observed. We compared these band changes, which correspond to carbamate intermediates [29, 30], with the changes in CO₂ fluxes across the membrane to find that they exhibit similar trends. Thus, we have direct spectroscopic evidence of the carrier saturation phenomenon. Our modeling and spectroscopic approaches are not limited to this particular membrane separation system and may be used to study other amine-based FTMs for CO₂ capture or FTMs for other types of separations such as olefin-paraffin separation, for example.

2. Experimental

2.1 Materials

N-vinylformamide (NVF, \geq 96% stabilized), citric acid (anhydrous lab grade), hydrochloric acid (HCl, 37%), and ethanol (denatured, anhydrous) were purchased from VWR. α,α' -azoisobutyronitrile (AIBN, 97%), silver nitrate (AgNO₃), and L-ascorbic acid were purchased from Sigma-Aldrich. Strong base anion-exchange resin (Purolite A600OH) was purchased from APS WATER. Polyvinylidene difluoride (PVDF) ultrafiltration substrate with a molecular weight cut off 100 kDa (pore size 10 nm) was kindly donated by the Phillip lab at the University of Notre Dame and originally supplied by Nanostone. PVDF was used as received. Porous polypropylene (PP) substrate was donated by Celgard. Celgard 2075 PP (20 μ m thick) was cleaned by soaking in ethanol for four hours followed by soaking in deionized water for four hours, and then dried in a fume hood overnight. All gas cylinders (purity of \geq 99.99%) were purchased from Airgas: Ar, CO₂, CH₄, and N₂.

2.2 Membrane fabrication

PVAm was synthesized following protocols described in our previous publications [29, 30]. 40 wt% N-vinylformamide aqueous solution was degassed with N₂, and 0.14 wt% 2,2′-azobis(2-methylpropionitrile) was added as the initiator. Polymerization was carried out at 50 °C for 3h. After polymerization, the polymer was hydrolyzed with 2M HCl at 70 °C for 5h under N₂. 3 wt% of the polymer aqueous solution was prepared and strong base anion-exchange resin was used to adjust the solution pH to 11. PVAm (3 wt%) aqueous solution was prepared and used to knife cast on the PVDF and PP support materials to fabricate PVAm membranes, with the PP-supported samples being compatible with transmission FTIR. To prepare the casting solution for the surface enhanced Raman scattering (SERS)-active membrane, 20.4 mg of silver nanoparticles were incorporated into 1 mL of 3 wt% PVAm aqueous solution to enhance the Raman signals [29]. All the membranes were dried overnight under ambient conditions. After drying, the PVAm-PVDF and PVAm/Ag NPs-PVDF membranes were installed in the SERS permeation cell with an active area of 2.2 cm². The PVAm-PP membrane was adhered to an aluminum disc with JB Weld Epoxy to install into the FTIR permeation cell with an active area of 0.79 cm².

2.3 PVAm membrane permeation experiments

Gas permeation measurements were conducted using an *operando* Raman spectroscopy permeation cell reported previously [29] where CO₂ and CH₄ were used as feed gases (10 mL/min total flow rate) and Ar was used as the sweep gas (148 mL/min flow rate). A high Ar sweep flow rate (148 mL/min) was necessary to keep the CO₂ concentration within the detection range of the flame ionization detector. To study the effect of CO₂ partial pressure on the membrane separation performance, the feed CO₂ partial pressure was varied from 2 to 99 kPa with 2.2 kPa H₂O and balance CH₄ at atmospheric pressure; this was achieved by adjusting the flow rates of the CO₂ and CH₄ gases, which were controlled by mass flow controllers (Aalborg MFC). The feed and sweep

gases were at ambient pressure for all experiments and flowed through humidifiers (Ace Glass) to introduce water vapor. The outlet gas composition of the permeate stream was analyzed using an SRI 8610C gas chromatograph (GC) equipped with a HayeSep D packed column and a flame ionization detector. All experiments were conducted at room temperature.

2.4 Operando surface enhanced Raman scattering (SERS) experiments

The *operando* surface enhanced Raman scattering (SERS) permeation cell was also used to observe the formation of carbamate species in PVAm from the interaction of CO₂ with the primary amine groups of PVAm. To enhance the intensity of vibrational bands associated with carbamate, Ag nanoparticles were involved in the PVAm aqueous solution prior to casting, as described in our previous publication [29]. The PVAm/Ag NPs-PVDF membrane was monitored using Raman spectroscopy while simultaneously measuring gas permeation rates on the same sample under identical operating conditions described in Section 2.3. All Raman spectroscopy measurements were performed using a Horiba iHR 320 Raman spectrometer with a 532 nm laser and a Horiba MicroHead 3000 fiber optic probe. The spectra were collected with an incident laser power of 9.8 mW and a 50x Nikon objective.

2.5 Operando transmission FTIR experiments

Operando transmission FTIR spectroscopy experiments were conducted using an operando transmission FTIR spectroscopy permeation cell reported in our previous work [30]. Spectroscopic measurements were performed at 22 °C and atmospheric pressure. The effect of feed composition was studied by using feed compositions of 2-97 kPa CO₂, 4.2 kPa H₂O, and balance N₂. The total feed flow rate was maintained at 37.5 mL/min and the Ar sweep flow rate was 10 mL/min. Transmission FTIR spectra were collected with a Bruker Tensor II spectrometer equipped with a

liquid nitrogen cooled mercury-cadmium-telluride (MCT) detector using a spectral resolution of 4 cm⁻¹ resolution, 1.5 min scans, and 6 mm aperture.

2.6 Scanning electron microscopy

Scanning electron microscopy (SEM) was used to determine the PVAm membrane thicknesses using a field emission scanning electron microscope (Magellan 400 FEI) equipped with a Bruker XFlash energy dispersive X-ray detector. Fig. 1 shows the SEM images of the PVAm membranes used in this study with thicknesses of (a) 1.7 μ m, (b) 2.6 μ m, and (c) 4.1 μ m, supported on PVDF. These membranes were used to study the effect of membrane thickness and feed CO₂ partial pressure on membrane performance in section 4.1.

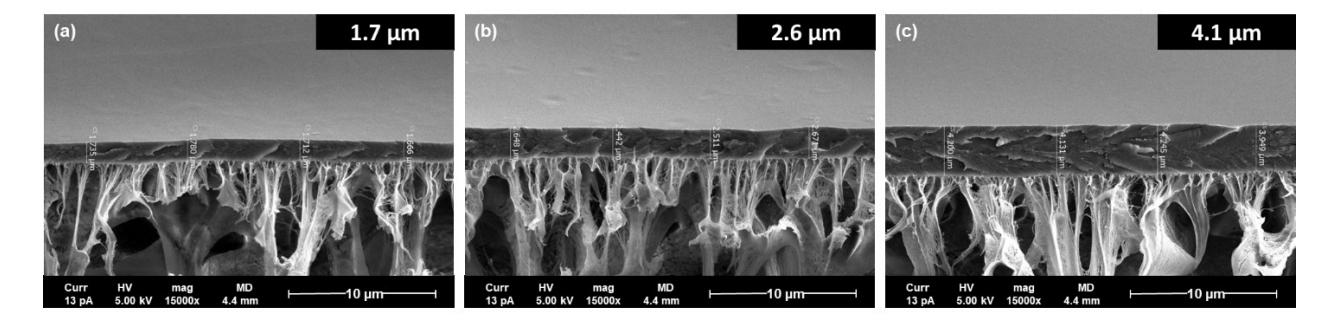


Fig. 1. SEM images of cross-sections of PVAm-PVDF membranes cast with different thickness gauges to obtain PVAm thicknesses of (a) 1.7 μ m; (b) 2.6 μ m; and (c) 4.1 μ m.

3. CO₂ transport mathematical model

We modeled the transport of CO₂ across PVAm by assuming that the transport occurred by two different transport mechanisms acting in parallel (see Fig. 2): solution-diffusion of neutral CO₂ and facilitated transport of CO₂ via carbamate, which we have previously identified [29, 30] as the main intermediate in the facilitated transport mechanism across PVAm. Thus, the total flux (mol/m²·s) of CO₂ across the membrane, J_{total} , is equal to the sum of the flux of CO₂ via facilitated transport, J_{FT} (mol/m²/s), and solution-diffusion, J_{SD} (mol/m²·s):

$$J_{total} = J_{SD} + J_{FT} \tag{1}$$

The flux of CO₂ across the membrane via solution-diffusion is given by equation (2) (see Appendix
1A for derivation) [48, 49]:

$$J_{SD} = \frac{k_{CO_2}}{x} \left(P_{CO_2, high} - P_{CO_2, low} \right)$$
 (2)

where k_{CO_2} represents the permeability of PVAm to CO₂ via solution diffusion (mol/m·s·Pa), x represents the membrane thickness (m), and $P_{CO_2,high}$ and $P_{CO_2,low}$ represent the CO₂ partial pressure (Pa) on the high CO₂ pressure and low CO₂ pressure side of the membrane, respectively. The flux of CO₂ across the membrane via facilitated transport of carbamate species ($NHCOO^-$) is given by equation (3) (see Appendix 1A for derivation):

$$J_{FT} = \frac{D_{NHCOO}C_{NH_2}}{x} \left(\frac{K_{eq}P_{CO_2,high}}{1 + K_{eq}P_{CO_2,high}} - \frac{K_{eq}P_{CO_2,low}}{1 + K_{eq}P_{CO_2,low}} \right)$$
(3)

where D_{NHCOO} represents the apparent diffusivity of carbamate species (m²/s) (note that the reactive amine carriers are fixed to the polymer chain and are not mobile; therefore, the carbamate species do not diffuse across the membrane but rather the carbamate species 'hop' from one amine site to another. Thus, D_{NHCOO} represents the apparent diffusivity of carbamate species hopping across the membrane); C_{NH_2} represents the concentration of amine sites in the membrane (mol/m³), which we assume to be constant throughout the volume of the membrane; K_{eq} (Pa⁻¹) represents the equilibrium constant for the formation of carbamate species from CO₂ and a free amine site (shown in Equation (4) and Fig. 2).

$$CO_2 + NH_2 \stackrel{K_{eq}}{\longleftrightarrow} NHCOO^- \cdots H^+ \tag{4}$$

212 Thus, the total flux across the membrane is given by:

213
$$J_{total} = \frac{k_{CO_2}}{x} \left(P_{CO_2, high} - P_{CO_2, low} \right) + \frac{D_{NHCOO}C_{NH_2}}{x} \left(\frac{K_{eq}P_{CO_2, high}}{1 + K_{eq}P_{CO_2, high}} - \frac{K_{eq}P_{CO_2, low}}{1 + K_{eq}P_{CO_2, low}} \right)$$
(5)

Unlike the DM transport model [37-44], which assumes there are holes in the polymer matrix that can adsorb solutes with no reaction occurring between the solutes and polymer matrix, our model considers the chemical reaction between the amine carriers on the polymer backbone and the solutes.

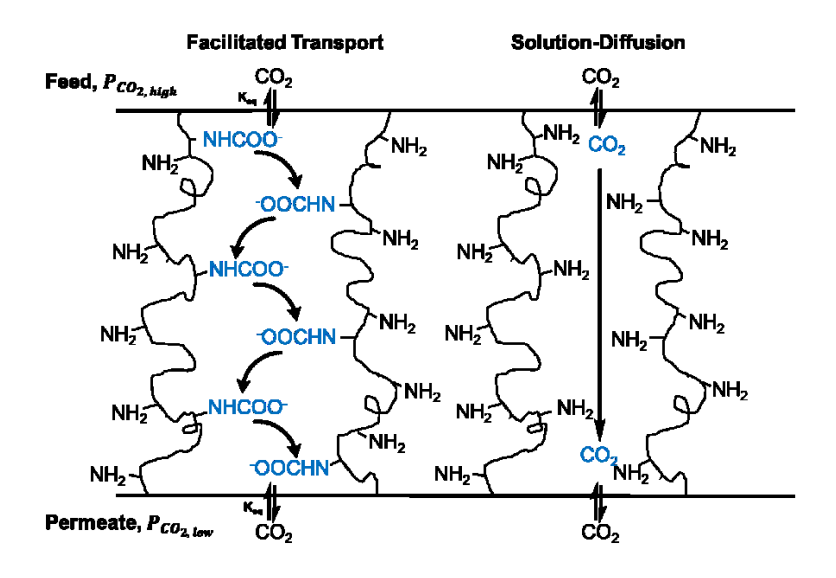


Fig. 2. Schematic representation of CO₂ transport across PVAm via facilitated transport of carbamate and solution-diffusion of CO₂.

There are three unknown adjustable parameters in the facilitated transport + solution-diffusion model: k_{CO_2} (the permeability of PVAm to CO₂ via solution diffusion); K_{eq} (the equilibrium constant for carbamate formation/decomposition); and the lumped parameter $D_{NHCOO}C_{NH_2}$. These three model parameters were fit to experimental CO₂ fluxes measured across PVAm membranes with three different thicknesses (1.7 μ m, 2.6 μ m, 4.1 μ m) and over nearly two decades of CO₂ feed partial pressures (2 to 99 kPa), for a total of 33 data points.

In order to obtain a good fit of the model to the experimental data, with parameters that make physical sense, it is important to provide good initial guesses for these adjustable parameters. The procedure for obtaining good initial guesses for these adjustable parameters is described in detail in Appendix 1B. To determine the values of k_{CO_2} , $D_{NHCOO}C_{NH_2}$, and K_{eq} that describe CO_2 transport in the PVAm membrane, a numerical solver (Excel Solver) was used to find the optimized values of k_{CO_2} , $D_{NHCOO}C_{NH_2}$, and K_{eq} that minimize the sum of the squared error between the measured CO_2 fluxes and the CO_2 fluxes predicted by the model (Equation (5)) over varied CO_2 partial pressure and membrane thickness. The computation is fast and is typically completed in 2-3 seconds.

4. Results and discussion

4.1 Mathematical modeling of CO₂ transport across PVAm

CO₂ permeation measurements across PVAm membranes were performed with a spectroscopic permeation cell reported in our previous work [29]. Pure PVAm membranes were prepared with thicknesses of 1.7 μm, 2.6 μm, and 4.1 μm to study the effect of both membrane thickness and feed CO₂ partial pressure (2-99 kPa) on membrane performance. The CO₂ flux across PVAm is plotted as a function of CO₂ partial pressure and membrane thickness in Fig. 3(a). The CO₂ flux increases continuously with increasing CO₂ partial pressure for all three membrane thicknesses; however, there is a distinct change in the slope of the CO₂ flux versus the feed CO₂ partial pressure at ~10 kPa. At pressures above ~10 kPa, the CO₂ flux increases roughly linearly with increasing CO₂ feed pressure. At pressures below ~10 kPa, the CO₂ flux increases nonlinearly with increasing CO₂ feed pressure. The change in the slope of the CO₂ flux versus CO₂ partial pressure is most likely due to a transition from a regime at low CO₂ partial pressures where

CO₂ transport occurs primarily via facilitated transport with a high CO₂ permeability to a regime at higher CO₂ partial pressures where the amine sites are saturated with CO₂ and the increase in the CO₂ flux with increasing CO₂ partial pressure is due to an increase in the solution-diffusion of CO₂ where the flux increase occurs less rapidly in comparison to below 10 kPa CO₂ where facilitated transport dominates.

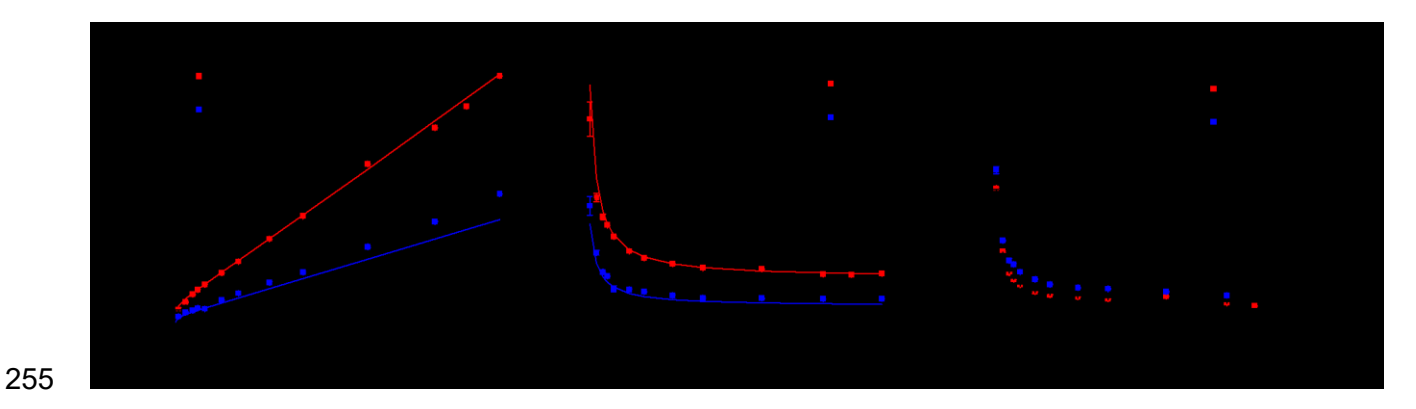


Fig. 3. Comparison of facilitated transport model (solid lines) with experimental data (squares) for (a) CO_2 flux; (b) apparent CO_2 permeance; and (c) CO_2/CH_4 selectivity as a function of the upstream CO_2 partial pressure with PVAm thicknesses of 1.7 μ m (red), 2.6 μ m (black), and 4.1 μ m (blue) at atmospheric pressure and room temperature.

In the literature [17, 18, 26, 50-52], CO₂ permeance is often used as a metric to evaluate the performance of FTMs such as PVAm. However, since CO₂ transport across FTMs occurs by facilitated transport and solution-diffusion in parallel, which are governed by different kinetic expressions, the CO₂ permeance in the literature is an 'apparent' CO₂ permeance that neglects the individual contributions of CO₂ facilitated transport and solution-diffusion. The apparent CO₂ permeance is defined as the total CO₂ flux across the membrane (J_{total}) divided by the CO₂ partial pressure driving force ($P_{CO_2,high} - P_{CO_2,low}$):

$$CO_2 apparent permeance = \frac{J_{total}}{P_{CO_2,high} - P_{CO_2,low}}$$
 (6)

Fig. 3(b) shows the apparent CO₂ permeance versus CO₂ partial pressure in the feed with PVAm membrane thicknesses of 1.7 μ m (red), 2.6 μ m (black), and 4.1 μ m (blue). We plot the apparent CO₂ permeance here for comparison to behavior reported in the literature [17, 18, 26, 50-52]. The apparent CO₂ permeance decreases with increasing PVAm thickness, as expected. At 2 kPa CO₂, the CO₂ permeance of PVAm is 340 \pm 30 GPU, 270 \pm 20 GPU, and 200 \pm 20 GPU with PVAm membrane thicknesses of 1.7 μ m, 2.6 μ m, and 4.1 μ m, respectively. The apparent CO₂ permeance decreases with increasing CO₂ partial pressure up to ~10-20 kPa and then remains relatively constant at 91.42 \pm 0.07 GPU (1.7 μ m), 61 \pm 9 GPU (2.6 μ m), and 46.8 \pm 0.6 GPU (4.1 μ m) for CO₂ feed pressures greater than 20 kPa. This trend of decreasing apparent CO₂ permeance with increasing CO₂ partial pressure is consistent with the trends reported in the literature [17, 18, 26, 50-52] and has been cited as the primary indicator of carrier saturation. The CO₂/CH₄ selectivity also decreased with increasing CO₂ partial pressure (see Fig. 3(c)).

The facilitated transport model described in Section 3 was fit to the experimental CO₂ fluxes in Fig. 3(a) to quantify the CO₂ flux that occurs via facilitated transport and solution diffusion and to extract kinetic and thermodynamic parameters associated with CO₂ transport across PVAm. The solver-optimized adjustable parameters k_{CO_2} , $D_{NHCOO}C_{NH_2}$, and K_{eq} were obtained with values of 150 ± 20 Barrer (1 Barrer = 3.35 × 10⁻¹⁶ mol/m·s·Pa), (4.5 ± 0.2) × 10⁻¹⁰ mol/m·s, and $(2 \pm 1) \times 10^{-3}$ Pa⁻¹, respectively. Using these solver-optimized values of the adjustable parameters, the CO₂ flux across PVAm was calculated as a function of CO₂ partial pressure (2-99 kPa) and PVAm membrane thickness (1.7 μ m, 2.6 μ m, 4.1 μ m) using Equation (5). As shown in Fig. 3(a), the model-calculated CO₂ fluxes (solid lines) fit the experimentally-measured CO₂ fluxes (data points) reasonably well, especially considering that only one set of parameters (k_{CO_2} , $D_{NHCOO}C_{NH_2}$, and K_{eq}) was used to model all of the experimental data over a

feed CO₂ partial pressure of 2 to 99 kPa, and with three different membrane thicknesses. Fig. S1 in the supporting information shows a parity plot of the experimental CO₂ flux versus the modeled CO₂ flux. The parity plot shows that the modeled CO₂ flux fits the experimental data well with a slope equal to 0.99 and an R² value of 1.00. The average absolute relative error (AARE) between the modeled CO₂ flux and the experimental CO₂ flux is 7%. The model-predicted CO₂ permeances, which were calculated using the model-predicted CO₂ fluxes and Equation (6), also fit the experimental CO₂ permeances reasonably well (see Fig. 3(b)). The AARE between the model and experimental CO₂ permeance is 6%.

The model indicates that the permeability of PVAm to carbamate via facilitated transport, which is given by the product of the parameters $D_{NHCOO}C_{NH_2}K_{eq}$, is 2200 ± 1200 Barrer. This is an order of magnitude greater than the permeability of PVAm to CO₂ via solution-diffusion (150 ± 20 Barrer). Comparing the K_{eq} ((2 ± 1) × 10⁻³, Pa⁻¹) extracted from the model with literature, we found no reported equilibrium constant for amine-based polymeric membranes and CO₂. The equilibrium constant associated with the interaction of CO₂ with amine sorbents has been reported in the literature; however, the equilibrium constants reported in the literature have different units. To better compare our model-extracted equilibrium constant with literature values, we nondimensionalized our equilibrium constant based on a method reported in the literature [53, 54] (Table S1). After nondimensionalization, our K_{eq} (200 ± 100) is between the equilibrium constant associated with the reaction of NH₃ and CO₂ (88.78) and the reaction of NH₂CH₃ with CO₂ (154400) [55, 56]. Thus, the equilibrium constant extracted from our model appears to be in a reasonable range.

The fraction of the total CO₂ flux that occurs via facilitated transport of carbamate species for each membrane (calculated by dividing the facilitated transport CO₂ flux by the total CO₂ flux)

is plotted in Fig. 4 as a function of feed CO_2 partial pressure. The fraction of the total CO_2 flux that occurs via facilitated transport of carbamate species decreases with increasing CO_2 partial pressure, from a value of ~ 0.8 at 2 kPa CO_2 to ~ 0.05 at 99 kPa CO_2 , and is mostly independent of the membrane thickness. This result shows that CO_2 transport across PVAm occurs primarily via facilitated transport at CO_2 feed pressures less than ~ 10 kPa (the fraction of CO_2 flux via facilitated transport $\sim 45\%$ at 10 kPa CO_2) and primarily through solution-diffusion at pressures greater than ~ 10 kPa; this transition is mostly independent of the membrane thickness.

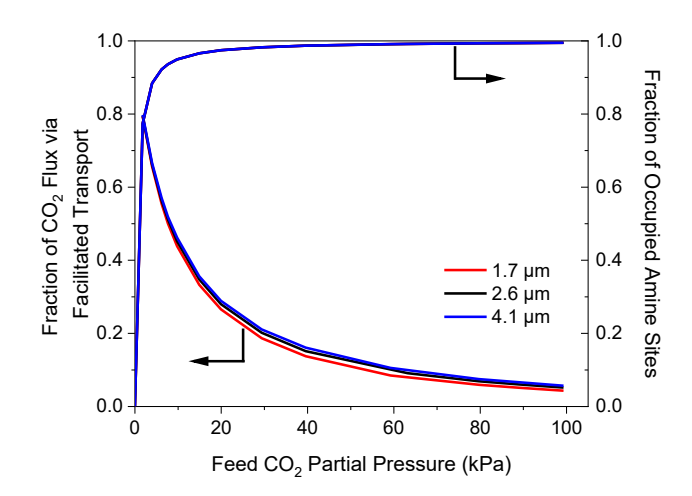


Fig. 4. Fraction of CO_2 flux via facilitated transport of carbamate (left axis) and fraction of amine sites occupied by CO_2 (carbamate) on the feed side of the membrane (right axis) as a function of the upstream CO_2 partial pressure for PVAm membranes with thicknesses of 1.7 μ m (red), 2.6 μ m (black), and 4.1 μ m (blue) during exposure to 2-99 kPa CO_2 , 2.2 kPa H_2O , and balance CH_4 at atmospheric pressure and room temperature.

The fraction of amine sites occupied by CO_2 on the feed side of the PVAm membrane, which was estimated using Eq. (A8) in Appendix 1A (in the Supporting Information) and the K_{eq} extracted from the model, is plotted as a function of CO_2 partial pressure and membrane thickness in Fig. 4 (right axis). The fraction of amine sites occupied by CO_2 on the feed side increases with

increasing feed CO_2 partial pressure reaching near full saturation around 10 kPa. As the K_{eq} value was assumed to be independent of the membrane thickness, the fraction of amine sites occupied by CO_2 on the feed side is also independent of the membrane thickness.

4.2 Operando spectroscopy study of PVAm membrane

Our model indicates that amine carrier saturation in PVAm occurs at a feed CO₂ partial pressure of about 10 kPa, with CO₂ transport primarily occurring via solution diffusion at CO₂ feed pressures higher than this. To determine whether this amine carrier saturation could be observed directly using *operando* spectroscopy, a SERS-active PVAm membrane was prepared by embedding plasmonic Ag NPs in the PVAm membrane. SERS spectra were collected at varying feed CO₂ partial pressures while CO₂ permeances and CO₂/CH₄ selectivities were measured simultaneously.

Fig. S2 compares SEM images of the PVAm membrane and the PVAm membrane with embedded silver nanoparticles (PVAm/Ag NPs), which shows that the thickness of the PVAm/Ag NPs membrane (~2.5 ± 0.2 μm) is similar to the pure PVAm membrane (~2.6 ± 0.1 μm). The permeation results (CO₂ flux, apparent CO₂ permeance, and CO₂/CH₄ selectivity) of the PVAm/Ag NPs are shown in Fig. 5 (red squares). As the CO₂ partial pressure increases, the apparent CO₂ permeance and CO₂ flux follow the same trend as the pure PVAm membrane; however, the CO₂ flux (Fig. 5(a)) and apparent CO₂ permeance (Fig. 5(b)) are slightly lower than the corresponding PVAm membrane for all conditions, which may be explained by the blocking of some pathways of CO₂ transport by Ag NPs [29]. However, the differences in the CO₂/CH₄ selectivity (Fig. 5(c)) are minimal. The experimentally measured CO₂ fluxes across the PVAm/Ag NPs membrane were also modeled using the facilitated-transport + solution-diffusion model (Equation (5)), and the

parameters extracted from the optimized model (see Table S2) are in good agreement with the results from PVAm membranes.

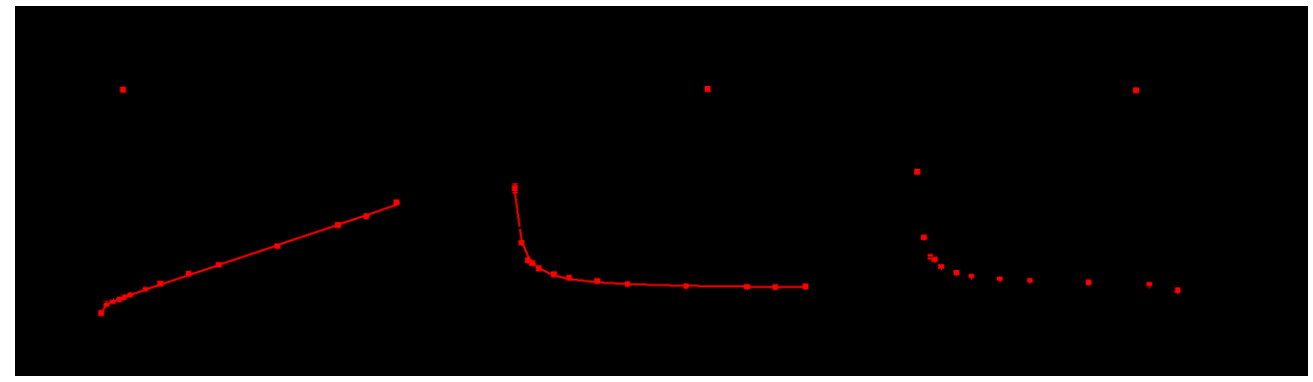


Fig. 5. Comparison of (a) CO₂ flux, (b) apparent CO₂ permeance, and (c) CO₂/CH₄ selectivity for the experimental data (squares) and the models (solid lines) as functions of the upstream CO₂ partial pressure for PVAm and PVAm/Ag NPs membranes during exposure to 2-99 kPa CO₂, 2.2 kPa H₂O, and balance CH₄ at atmospheric pressure and room temperature.

The *operando* Raman spectra collected during exposure to varying CO₂ partial pressures (2-99 kPa) are shown in Fig. 6(a). There are several Raman peaks in the 1076-1693 cm⁻¹ region, which we have previously assigned to ammonium carbamate species [29, 30], that increase in intensity with increasing CO₂ partial pressure but do not change position. To better visualize the variation of these Raman peak intensities with CO₂ partial pressure, the peak areas in the 1076-1693 cm⁻¹ range were integrated and normalized by the maximum integral area observed at a CO₂ partial pressure of 99 kPa. The normalized Raman integral areas are plotted as a function of CO₂ partial pressure in Fig. 6(b) (blue squares). The normalized integral area of the Raman peaks in the 1076-1693 cm⁻¹ range increases with increasing feed CO₂ partial pressure up to ~10 kPa CO₂. Above ~10 kPa CO₂, the intensity of these peaks remains relatively constant. Because these peaks are associated with carbamate species, this observation indicates that the primary amine sites of PVAm are saturated with CO₂ (carbamate) at CO₂ partial pressures above ~10 kPa. This is the first direct observation of the carrier saturation phenomenon in amine-functionalized facilitated

transport membranes, to our knowledge. The fraction of amine sites occupied by CO_2 on the feed side of PVAm, estimated from model predictions as described above, is also plotted versus CO_2 partial pressure in Fig. 6(b) (black line) for comparison to the normalized integral area of the Raman peaks in the 1076-1693 cm⁻¹ range. There appears to be a strong correlation between the model-predicted fraction of amine sites occupied by CO_2 and the normalized integral area of the Raman peaks associated with carbamate; both increase sharply with increasing CO_2 partial pressure and then saturate at \sim 10 kPa CO_2 . This correlation further validates the accuracy of the facilitated-transport + solution-diffusion model.

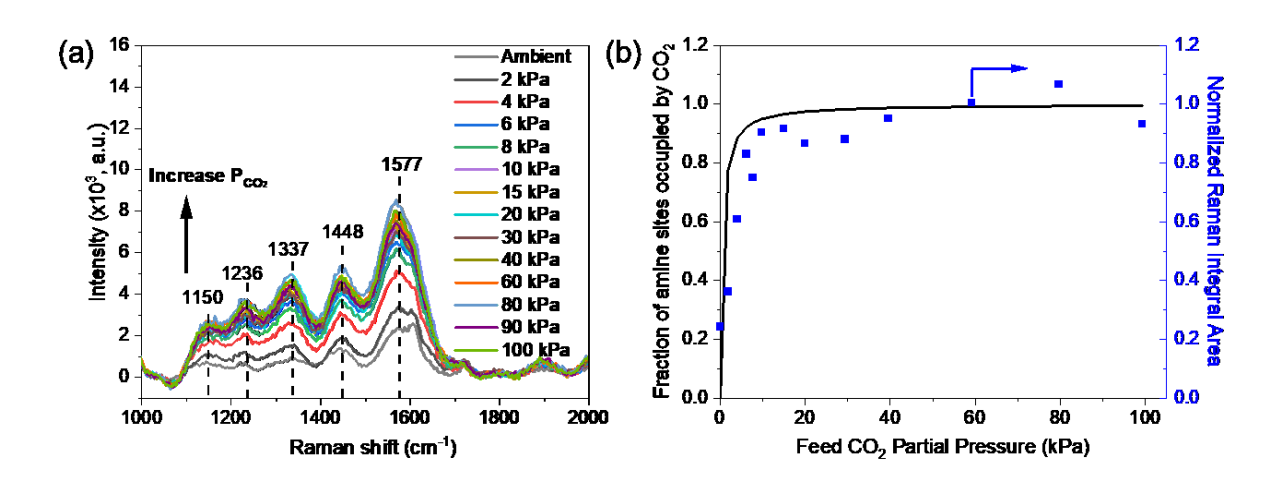


Fig. 6. (a) *Operando* Raman spectra as a function of CO₂ partial pressure during exposure to humidified CO₂/CH₄ with 2-99 kPa CO₂, 2.2 kPa H₂O, and balance CH₄ at atmospheric pressure and room temperature. (b) Fraction of amine sites occupied by CO₂ on the feed side of PVAm from model predictions (black line), and the normalized integral area of the Raman peaks between 1076-1694 cm⁻¹ (blue squares), versus feed CO₂ partial pressure.

As transmission FTIR and Raman spectroscopy are complementary techniques, in-situ transmission FTIR spectroscopy was also used to observe the saturation of the primary amine

groups of PVAm with CO₂ (carbamate). Fig. 7(a) shows the *operando* transmission FTIR spectra collected during exposure of PVAm to humidified CO₂/N₂ gas mixtures over a range of CO₂ feed partial pressures from 0 to 97 kPa. A comparison of Raman and FTIR band assignments is given in Table S3 with references to literature. The Raman and FTIR band positions are consistent with each other and with carbamate species, which further supports our assignment of these peaks to carbamate species. Similar to the *operando* Raman results, the *operando* transmission FTIR spectra also show that the intensity of all FTIR bands associated with carbamate increase rapidly up to ~10 kPa CO₂ and these band intensities change minimally with further increasing CO₂ partial pressure. Similar to the previous discussion related to *operando* Raman spectroscopy, the FTIR spectra were integrated from 1112-1725 cm⁻¹, normalized, and plotted against the CO₂ partial pressure in Fig. 7(b). The normalized FTIR integrated area also correlates well with the fraction of amine sites occupied by CO₂ on the feed side, also plotted in Fig. 7(b), which further validates our combined modeling and spectroscopic approach to quantitatively and mechanistically describe CO₂ facilitated transport across PVAm.

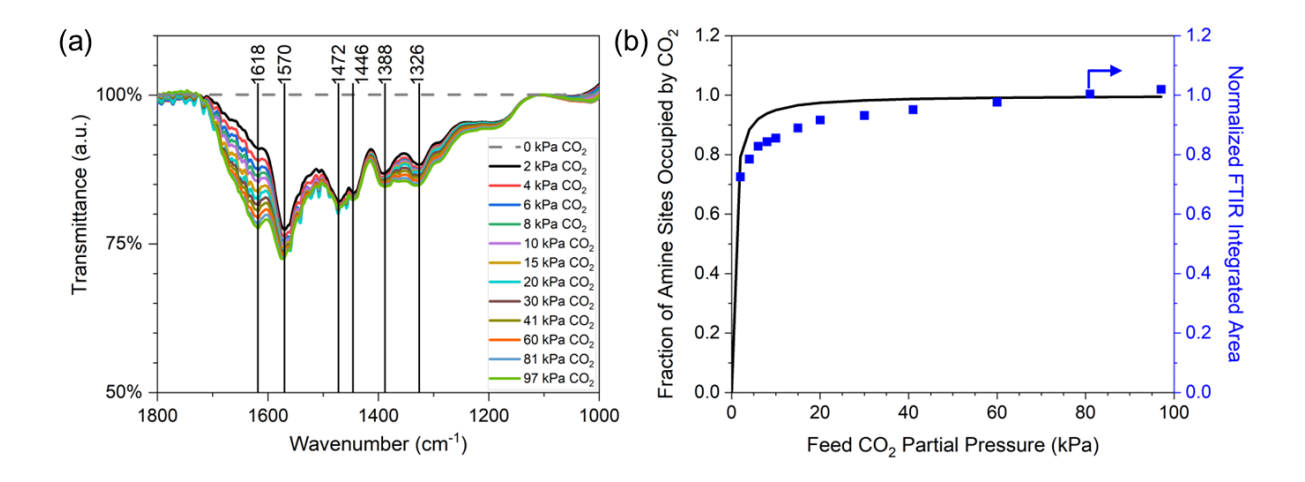


Fig. 7. (a) *Operando* transmission FTIR spectra of PVAm/PP during exposure to humidified CO₂/N₂ with 2-97 kPa CO₂, 4.2 kPa H₂O, and balance N₂ at atmospheric pressure and 22 °C. (b) Fraction of amine sites occupied by CO₂ estimated from model predictions (black line) and the integral area of the FTIR spectra (blue squares) in the 1112-1725 cm⁻¹, versus CO₂ partial pressure.

The CO₂ partial pressure at which the carbamate Raman peaks (Fig. 6) and FTIR peaks (Fig. 7) saturate (~10 kPa CO₂) also coincides with a distinct change in the CO₂ permeation behavior. CO₂ transport occurs primarily via facilitated transport of carbamate species across the membrane at CO₂ partial pressures below ~10 kPa (Fig. 4). The CO₂ flux (Fig. 3(a)) varies nonlinearly, and the CO₂ permeance (Fig. 3(b)) decreases, with increasing CO₂ partial pressure as the amine sites become increasingly occupied by CO₂ (carbamate) up to ~10 kPa CO₂. Above ~10 kPa CO₂, the amine sites are completely saturated and CO₂ transport occurs primarily via solution-diffusion of CO₂. Consequently, the CO₂ flux increases linearly, and the CO₂ permeance is roughly constant, with increasing CO₂ partial pressure. Thus, the greatest benefits of facilitated transport membranes occur at low CO₂ partial pressures (less than ~10 kPa for PVAm).

5. Conclusion

A simple mathematical expression for CO₂ transport through PVAm membrane was derived and fit to experimental data of CO₂/CH₄ gas separation in PVAm-PVDF membranes with different thicknesses at varied CO₂ partial pressures. The comparison between experimental and model-predicted CO₂ fluxes and permeances indicates a good fit of the model to the experimental data. The model gives quantitative information about key thermodynamic and kinetic parameters associated with CO₂ transport across amine-functionalized membranes, such as CO₂ solution diffusion permeability (k_{CO_2}), CO₂ facilitated transport permeability ($D_{NHCOO}C_{NH_2}K_{eq}$), and carbamate formation/decomposition equilibrium constant (K_{eq}). PVAm/Ag NPs-PVDF and PVAm-PP membranes were also prepared and tested with our spectroscopic permeation cells to monitor the formation of carbamate species in the PVAm membrane from the interaction of the

primary amine groups of PVAm with CO₂. We observed that both the Raman bands and the FTIR bands associated with carbamate species increased with increasing feed CO₂ partial pressure until saturation was observed at a CO₂ partial pressure of ~10 kPa. Our combined mathematical modeling and spectroscopic approach provides direct spectroscopic evidence of the carrier saturation phenomenon in amine-functionalized polymer membranes for the first time, to our knowledge. Further, this work demonstrates that CO₂ transport across PVAm occurs primarily via facilitated transport of carbamate species at CO₂ partial pressures below ~10 kPa CO₂, and primarily via solution-diffusion of CO₂ at pressures above ~10 kPa CO₂ where the primary amine groups of PVAm are saturated with CO₂ (carbamate).

The mathematical modeling approach reported in this work can also be applied to other amine-functionalized membranes for CO₂ separation and other types of facilitated transport membranes, such as silver-functionalized polymer membranes for olefin-paraffin separation. The model parameters extracted from this work using PVAm cannot be used to predict CO₂ transport across other membrane compositions, because the adjustable parameters in the model are intrinsic material properties that depend on the membrane composition. However, this modeling approach allows one to extract more detailed, and more fundamental, quantitative information about the CO₂ transport process than is typically reported in the literature. This leads to greater fundamental understanding of the CO₂ transport process, which is particularly important for establishing reliable structure-function relationships, and enables a more rational design of high-performance CO₂ separation membranes than is possible with current trial-and-error approaches to membrane development. Therefore, this model will be a valuable tool for future design and optimization of other CO₂ separation systems in more efficient process configurations.

6. Nomenclature

- $C_{CO_2,high}$: concentration of CO₂ dissolved on the high CO₂ pressure side of the membrane
- $C_{CO_2,low}$: concentration of CO₂ dissolved on the low CO₂ pressure side of the membrane
- C_{NH_2} : concentration of amine sites in the membrane
- C_{NHCOO} : concentration of carbamate species in the membrane
- D_{CO_2} : CO₂ diffusion coefficient
- D_{NHCOO} : apparent diffusivity of carbamate species hopping across the membrane
- S_{CO_2} : solubility of CO₂ in the membrane
- $P_{CO_2,high}$: CO₂ partial pressure on the high-pressure side of the membrane
- $P_{CO_2,low}$: CO₂ partial pressure on the low-pressure side of the membrane
- k_{CO_2} : permeability of CO₂ via solution diffusion
- J_{FT} : facilitated transport flux
- J_{SD} : solution-diffusion flux
- J_{total} : total flux of CO₂ across the membrane
- K_{eq} : equilibrium constant for the formation of carbamate species from CO₂ and a free amine site
- θ_{high} : fraction of amine sites occupied by CO₂ on the high-pressure side of the membrane

476 θ_{low} : fraction of those amine sites occupied by CO₂ on the low-pressure side of the membrane *x*: membrane thickness 477 478 479 **Author contributions** 480 Hui Xu: Investigation, formal analysis, writing-original draft, visualization; Sarah Pate: Investigation, formal analysis, writing-original draft; Casey O'Brien: Conceptualization, writing-481 482 review & editing, supervision, project administration. 483 **Declaration of Competing Interest** The authors declare that they have no known competing financial interests or personal 484 relationships that could have appeared to influence the work reported in this paper. 485 486 **Data availability** 487 Data will be made available on request. 488 **Acknowledgments** This work was funded through U.S. national Science Foundation CAREER award [CBET-489 490 2144362]. We also acknowledgethe Patrick and Jana Eilers Graduate Student Fellowship for 491 support. We thank Professor William Phillip's group for providing the PVDF support membranes. We also thank Notre Dame Integrated Imaging Facility (NDIIF) for the SEM analysis. 492 493 494 References [1] Z. Tong, W.S.W. Ho, Facilitated Transport Membranes for CO₂ Separation and Capture, Sep. Sci. 495 496 Technol. 52(2) (2017) 156-167. https://doi.org/10.1080/01496395.2016.1217885.

- 497 [2] R.L. Siegelman, P.J. Milner, E.J. Kim, S.C. Weston, J.R. Long, Challenges and Opportunities for 498 Adsorption-Based CO₂ Capture from Natural Gas Combined Cycle Emissions, Energy Environ. Sci. 12(7) 499 (2019) 2161-2173. https://doi.org/10.1039/C9EE00505F.
- [3] A.S. Bhown, B.C. Freeman, Analysis and Status of Post-Combustion Carbon Dioxide Capture 500 501 Technologies, Environ, Sci. Technol. 45(20) (2011) 8624-8632, https://doi.org/10.1021/es104291d.
- 502 [4] R.S. Haszeldine, Carbon Capture and Storage: How Green Can Black Be?, Science 325(5948) (2009) 503 1647-1652. https://doi.org/doi:10.1126/science.1172246.
- 504 [5] E. National Academies of Sciences, Medicine, D.o.E. Studies, Life, O.S. Board, B.o.C.S.a. Technology,
- 505 B.o.E.S.a. Resources, B.o.A. Resources, Natural, B.o.E. Systems, Environmental, B.o.A.S.a. Climate,
- 506 C.o.D.a.R.A.f.C.D.R. Sequestration, Reliable, Negative Emissions Technologies and Reliable
- 507 Sequestration: A Research Agenda, Washington, D.C: National Academies Press2019. 508 https://doi.org/10.17226/25259.
- 509 [6] R.W. Baker, B.T. Low, Gas Separation Membrane Materials: A Perspective, Macromolecules 47(20) 510 (2014) 6999-7013. https://doi.org/10.1021/ma501488s.
- [7] J. Guozhao, Z. Ming, Membrane Separation Technology in Carbon Capture, in: Y. Yongseung (Ed.), 511
- 512 Recent Advances in Carbon Capture and Storage, IntechOpen, Rijeka, 2017, p. Ch. 3. 513 https://doi.org/10.5772/65723.
- 514 [8] Z. Dai, S. Fabio, N. Giuseppe Marino, C. Riccardo, L. Deng, Field Test of a Pre-pilot Scale Hollow 515 Fiber Facilitated Transport Membrane for CO₂ Capture, Int. J. Greenh. Gas Control. 86 (2019) 191-200.
- 516 https://doi.org/https://doi.org/10.1016/j.ijggc.2019.04.027.
- 517 [9] M. Sandru, T.-J. Kim, W. Capala, M. Huijbers, M.-B. Hägg, Pilot Scale Testing of Polymeric
- 518 Membranes for CO₂ Capture from Coal Fired Power Plants, Energy Procedia 37 (2013) 6473-6480. 519 https://doi.org/https://doi.org/10.1016/j.egypro.2013.06.577.
- 520 [10] M.B. Hägg, A. Lindbråthen, X. He, S.G. Nodeland, T. Cantero, Pilot Demonstration-Reporting on CO₂
- 521 Capture from a Cement Plant Using Hollow Fiber Process, Energy Procedia 114 (2017) 6150-6165. 522 https://doi.org/https://doi.org/10.1016/j.egypro.2017.03.1752.
- 523 [11] W. Salim, V. Vakharia, Y. Chen, D. Wu, Y. Han, W.S.W. Ho, Fabrication and Field Testing of Spiral-
- 524 Wound Membrane Modules for CO₂ Capture from Flue Gas, J. Membr. Sci. 556 (2018) 126-137. 525 https://doi.org/https://doi.org/10.1016/j.memsci.2018.04.001.
- 526 [12] Y. Cai, Z. Wang, C. Yi, Y. Bai, J. Wang, S. Wang, Gas Transport Property of Polyallylamine-527 Poly(vinyl alcohol)/Polysulfone Composite Membranes, J. Membr. Sci. 310(1) (2008) 184-196.
- 528 https://doi.org/https://doi.org/10.1016/j.memsci.2007.10.052.
- 529 [13] S.E. Kentish, C.A. Scholes, G.W. Stevens, Carbon Dioxide Separation Through Polymeric Membrane 530 Systems for Flue Gas Applications, Recent Pat. Chem. Eng. 1 (2008) 52-66.
- 531 [14] Y. Han, W.S.W. Ho, Recent Advances in Polymeric Membranes for CO₂ Capture, Chin. J. Chem. Eng. 532 26(11) (2018) 2238-2254. https://doi.org/https://doi.org/10.1016/j.cjche.2018.07.010.
- 533 [15] A. Klemm, Y.-Y. Lee, H. Mao, B. Gurkan, Facilitated Transport Membranes With Ionic Liquids for 534 CO₂ Separations, Front. Chem. 8 (2020). https://doi.org/10.3389/fchem.2020.00637.
- 535 [16] H. Guo, J. Wei, Y. Ma, J. Deng, S. Yi, B. Wang, L. Deng, X. Jiang, Z. Dai, Facilitated Transport
- 536 Membranes for CO₂/CH₄ Separation - State of the Art, Advanced Membranes 2 (2022) 100040. 537 https://doi.org/https://doi.org/10.1016/j.advmem.2022.100040.
- 538 [17] Y. Han, W.S.W. Ho, Design of Amine-Containing CO₂-Selective Membrane Process for Carbon
- 539 Capture from Flue Gas, Ind. Eng. Chem. Res. (2020)5340-5350. 59(12)
- 540 https://doi.org/10.1021/acs.iecr.9b04839.
- 541 [18] M.S.A. Rahaman, L. Zhang, L.-H. Cheng, X.-H. Xu, H.-L. Chen, Capturing Carbon Dioxide from Air
- 542 Using a Fixed Carrier Facilitated Transport Membrane, RSC Adv. 2(24) (2012) 9165-9172.
- 543 https://doi.org/10.1039/C2RA20783D.
- 544 [19] Y. Zhang, Z. Wang, S. Wang, Novel Fixed-Carrier Membranes for CO₂ Separation, J. Appl. Polym.
- 545 Sci. 86(9) (2002) 2222-2226. https://doi.org/https://doi.org/10.1002/app.11228.
- 546 [20] L. Deng, T.-J. Kim, M.-B. Hägg, Facilitated Transport of CO₂ in Novel PVAm/PVA Blend Membrane,
- 547 J. Membr. Sci. 340(1) (2009) 154-163. https://doi.org/https://doi.org/10.1016/j.memsci.2009.05.019.

- 548 [21] Y.-Y. Lee, B. Gurkan, Graphene Oxide Reinforced Facilitated Transport Membrane with Poly(ionic
- 549 liquid) and Ionic Liquid Carriers for CO₂/N₂ Separation, J. Membr. Sci. 638 (2021) 119652.
- 550 https://doi.org/https://doi.org/10.1016/j.memsci.2021.119652.
- 551 [22] Y.-Y. Lee, N.P. Wickramasinghe, R. Dikki, D.L. Jan, B. Gurkan, Facilitated Transport Membrane with
- Functionalized Ionic Liquid Carriers for CO₂/N₂, CO₂/O₂, and CO₂/Air Separations, Nanoscale (2022).
- 553 <u>https://doi.org/10.1039/D2NR03214G</u>.
- 554 [23] Y. Han, W.S.W. Ho, Polymeric Membranes for CO₂ Separation and Capture, J. Membr. Sci. 628 (2021)
- 555 119244. https://doi.org/https://doi.org/10.1016/j.memsci.2021.119244.
- 556 [24] Y. Han, D. Wu, W.S.W. Ho, Simultaneous Effects of Temperature and Vacuum and Feed Pressures
- on Facilitated Transport Membrane for CO₂/N₂ Separation, J. Membr. Sci. 573 (2019) 476-484.
- 558 <u>https://doi.org/https://doi.org/10.1016/j.memsci.2018.12.028.</u>
- 559 [25] A. Matsuoka, A. Otani, E. Kamio, H. Matsuyama, A Gradient Viscosity Model for Estimating CO₂
- Permeability of Amino Acid Ionic Liquid-based Facilitated Transport Membrane, Sep. Purif. Technol. 280
- 561 (2022) 119847. https://doi.org/https://doi.org/10.1016/j.seppur.2021.119847.
- 562 [26] B. Belaissaoui, E. Lasseuguette, S. Janakiram, L. Deng, M.C. Ferrari, Analysis of CO₂ Facilitation
- Transport Effect through a Hybrid Poly(Allyl Amine) Membrane: Pathways for Further Improvement,
- Membranes (Basel) 10(12) (2020). https://doi.org/10.3390/membranes10120367.
- [27] C. Ma, M. Wang, Z. Wang, M. Gao, J. Wang, Recent progress on thin film composite membranes for
- 566 CO₂ separation, J. CO₂ Util. 42 (2020) 101296.
- 567 [28] Y. Chen, W.W. Ho, High-Molecular-Weight Polyvinylamine/Piperazine Glycinate Membranes for
- 568 CO₂ Capture from Flue Gas, J. Membr. Sci. 514 (2016) 376-384.
- [29] H. Xu, J. Easa, S.G. Pate, R. Jin, C.P. O'Brien, Operando Surface-Enhanced Raman-Scattering (SERS)
- 570 for Probing CO₂ Facilitated Transport Mechanisms of Amine-Functionalized Polymeric Membranes, ACS
- 571 Appl. Mater. Interfaces 14(13) (2022) 15697-15705. https://doi.org/10.1021/acsami.2c02769.
- 572 [30] S.G. Pate, H. Xu, C.P. O'Brien, Operando Observation of CO₂ Transport Intermediates in
- Polyvinylamine Facilitated Transport Membranes, and the Role of Water in the Formation of Intermediates,
- 574 Using Transmission FTIR Spectroscopy, J. Mater. Chem. A 10(8) (2022) 4418-4427.
- 575 https://doi.org/10.1039/D1TA10015G.
- 576 [31] Q. Yang, Q. Lin, S. Sammarchi, J. Li, S. Li, D. Wang, Water Vapor Effects on CO₂ Separation of
- 577 Amine-Containing Facilitated Transport Membranes (AFTMs) Module: Mathematical Modeling Using
- 578 Tanks-In-Series Approach, Greenh. Gases: Sci. Technol. 11(1) (2021) 52-68
- 579 https://doi.org/https://doi.org/https://doi.org/10.1002/ghg.2031.
- 580 [32] Q. Yang, Q. Lin, X. Liang, Modeling CO₂ Separation on Amine-Containing Facilitated Transport
- Membranes (AFTMs) by Linking Effects of Relative Humidity, Temperature, and Pressure, Int. J. Greenh.
- 582 Gas Control. 108 (2021) 103327. https://doi.org/https://doi.org/10.1016/j.ijggc.2021.103327.
- 583 [33] R. Rea, M.G.D. Angelis, M.G. Baschetti, Models for Facilitated Transport Membranes: A Review,
- 584 Membranes 9(2) (2019) 26. https://doi.org/10.3390/membranes9020026.
- 585 [34] X. He, Polyvinylamine-Based Facilitated Transport Membranes for Post-Combustion CO₂ Capture:
- 586 Challenges and Perspectives from Materials to Processes, Engineering 7(1) (2021) 124-131.
- 587 https://doi.org/https://doi.org/10.1016/j.eng.2020.11.001.
- 588 [35] J.S. Schultz, J.D. Goddard, S.R. Suchdeo, Facilitated Transport via Carrier-Mediated Diffusion in
- 589 Membranes: Part I. Mechanistic Aspects, Experimental Systems and Characteristic Regimes, AIChE J. 20(3)
- 590 (1974) 417-445. https://doi.org/https://doi.org/10.1002/aic.690200302.
- [36] Y. Han, W.S.W. Ho, Moving Beyond 90% Carbon Capture by Highly Selective Membrane Processes,
- 592 Membranes 12(4) (2022) 399.
- [37] I. Langmuir, The Adsorption of Gases on Plane Surfaces of Glass, Mica and Platinum, J. Am. Chem.
- 594 Soc. 40(9) (1918) 1361-1403. https://doi.org/10.1021/ja02242a004.
- 595 [38] R.I. Masel, Principles of Adsorption and Reaction on Solid Surfaces, 1996.
- 596 [39] M. Yoshikawa, T. Ezaki, K. Sanui, N. Ogata, Selective Permeation of Carbon Dioxide Through
- 597 Synthetic Polymer Membranes Having Pyridine Moiety as a Fixed Carrier, J. Appl. Polym. Sci. 35(1) (1988)
- 598 145-154. https://doi.org/https://doi.org/10.1002/app.1988.070350113.

- 599 [40] M. Yoshikawa, K. Fujimoto, H. Kinugawa, T. Kitao, Y. Kamiya, N. Ogata, Specialty Polymeric
- 600 Membranes. V. Selective Permeation of Carbon Dioxide Through Synthetic Polymeric Membranes Having
- 601 2-(N,N-Dimethyl)Aminoethoxycarbonyl Moiety, J. Appl. Polym. Sci. 58(10) (1995) 1771-1778.
- 602 https://doi.org/https://doi.org/10.1002/app.1995.070581015.
- 603 [41] R.M. Barrer, Diffusivities in Glassy Polymers for the Dual Mode Sorption Model, J. Membr. Sci. 18 (1984) 25-35. https://doi.org/https://doi.org/10.1016/S0376-7388(00)85023-1. 604
- 605 [42] R.D. Noble, Analysis of Facilitated Transport with Fixed Site Carrier Membranes, J. Membr. Sci. 50(2)
- 606 (1990) 207-214. https://doi.org/https://doi.org/10.1016/S0376-7388(00)80316-6.
- 607 [43] R.D. Noble, Facilitated Transport Mechanism in Fixed Site Carrier Membranes, J. Membr. Sci. 60(2)
- 608 (1991) 297-306. https://doi.org/https://doi.org/10.1016/S0376-7388(00)81541-0.
- 609 [44] R.D. Noble, Generalized Microscopic Mechanism of Facilitated Transport in Fixed Site Carrier
- 610 Membranes, J. Membr. Sci. 75(1) (1992) 121-129. https://doi.org/https://doi.org/10.1016/0376-
- 611 7388(92)80011-8.
- [45] W. Henry, J. Banks, Experiments on the Quantity of Gases Absorbed by Water, at Different 612
- 613 Temperatures, and under Different Pressures, Abstracts of the Papers Printed in the Philosophical
- Transactions of the Royal Society of London 1 (1832) 103-104. https://doi.org/doi:10.1098/rspl.1800.0063. 614
- 615 [46] R. Rea, M.G. De Angelis, M.G. Baschetti, Models for Facilitated Transport Membranes: A Review,
- 616 Membranes 9(2) (2019) 26.
- [47] E.L. Cussler, R. Aris, A. Bhown, On the Limits of Facilitated Diffusion, J. Membr. Sci. 43(2) (1989) 617
- 618 149-164. https://doi.org/https://doi.org/10.1016/S0376-7388(00)85094-2.
- 619 [48] A.T. Conlisk, Essentials of Micro- and Nanofluidics: with Applications to the Biological and Chemical
- 620 Sciences, Cambridge, New York: Cambridge University Press, 2013.
- 621 [49] C. Schaschke, Fick's First Law of Diffusion, Oxford University Press, 2014.
- 622 [50] B. Belaissaoui, E. Lasseuguette, S. Janakiram, L. Deng, M.-C. Ferrari, Analysis of CO₂ Facilitation
- 623 Transport Effect through a Hybrid Poly(Allyl Amine) Membrane: Pathways for Further Improvement, 624 Membranes 10(12) (2020) 367.
- 625 [51] J. Liao, Z. Wang, C. Gao, S. Li, Z. Qiao, M. Wang, S. Zhao, X. Xie, J. Wang, S. Wang, Fabrication of
- 626 High-Performance Facilitated Transport Membranes for CO₂ Separation, Chem. Sci. 5(7) (2014) 2843-
- 627 2849. https://doi.org/10.1039/C3SC53334D.
- 628 [52] C. Zhang, Z. Wang, Y. Cai, C. Yi, D. Yang, S. Yuan, Investigation of Gas Permeation Behavior in
- 629 Facilitated Transport Membranes: Relationship between Gas Permeance and Partial Pressure, Chem. Eng.
- 630 J. 225 (2013) 744-751. https://doi.org/https://doi.org/10.1016/j.cej.2013.03.100.
- 631 [53] X. Zhou, X. Zhou, The Unit Problem in the Thermodynamic Calculation of Adsorption Using the
- 632 Langmuir Equation, Chem Eng Commun 201(11) (2014)1459-1467. 633 https://doi.org/10.1080/00986445.2013.818541.
- 634
- [54] M. Özcan, Why Equilibrium Constants Are Unitless, J. Phys. Chem. Lett. 13(15) (2022) 3507-3509.
- 635 https://doi.org/10.1021/acs.jpclett.2c00314.
- 636 [55] G. Bresciani, L. Biancalana, G. Pampaloni, F. Marchetti, Recent Advances in the Chemistry of Metal
- 637 Carbamates, Molecules 25(16) (2020) 3603. https://doi.org/10.3390/molecules25163603.
- 638 [56] D.B. Dell'Amico, F. Calderazzo, L. Labella, F. Marchetti, G. Pampaloni, Converting Carbon Dioxide
- 639 Chemical Carbamato Derivatives. Reviews 103(10) (2003)3857-3898.
- 640 https://doi.org/10.1021/cr940266m.

641 642